SAND2020-2719R

CASL-U-2020-1938-000

Consortium for Advanced Simulation of LWRs

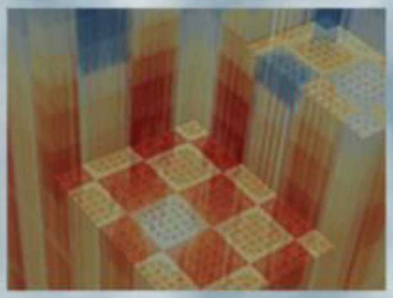

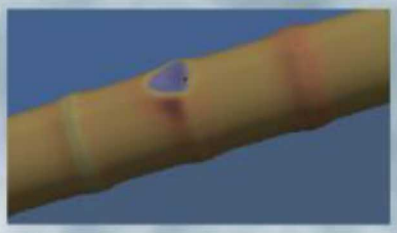

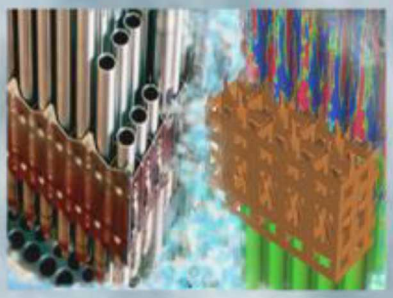

FY20 Improvements to CTF Code Verification and Unit Testing

Nathan W. Porter[1], Robert K. Salko[2], and Martin Pilch[3]

[1]Sandia National Laboratories
[2]Oak Ridge National Laboratory
[3]MPilch Consulting

15 February 2020

Sandia National Laboratories is a multimission laboratory managed and operated by National Technology & Engineering Solutions of Sandia, LLC, a wholly owned subsidiary of Honeywell International Inc., for the U.S. Department of Energy's National Nuclear Security Administration under contract DE-NA0003525.

Revision Log

Revision	Date	Affected Pages	Revision Description
0	15 February 2020	All	Initial Release

Document pages that are:

Export Controlled:	None
IP/Proprietary/NDA Controlled:	None
Sensitive Controlled:	None
Unlimited:	All

Executive Summary

In 2010, the U.S. Department of Energy created its first Energy Innovation Hub, which focuses on improving Light Water Reactors (LWRs) through Modeling and Simulation. This hub, named the Consortium for the Advanced Simulation of LWRs (CASL), attempts to characterize and understand LWR behavior under normal operating conditions and use any gained insights to improve their efficiency. In collaboration with North Carolina State University (NCSU), CASL has worked extensively on the thermal-hydraulic subchannel code Coolant Boiling in Rod Arrays–Three Field (COBRA-TF). The NCSU/CASL version of COBRA-TF has been rebranded as CTF.

This document focuses on code verification test problems that ensure CTF converges to the correct answer for the intended application. The suite of code verification tests are mapped to the underlying conservation equations of CTF, and significant gaps are addressed. Convergence behavior and numerical errors are quantified for each of the tests. Tests that converge at the correct rate to the corresponding analytic solution are incorporated into the CTF automated regression suite. A new verification utility is created for this purpose, which enables code verification by generalizing the process. For problems that do not behave correctly, the results are reported but the problem is not included in the regression suite.

In addition to verification studies, this document also quantifies the existing tests of constitutive models. A few existing gaps are addressed by adding new unit tests.

Contents

List of Figures

List of Tables

1. Introduction

Coolant Boiling in Rod Arrays–Three Field (COBRA-TF) is a thermal–hydraulic subchannel code for Light Water Reactor (LWR) core analysis. It was initially developed in the early 1980's at Pacific Northwest National Laboratory (PNNL) to model Loss of Coolant Accidents (LOCAs) [1]. The code has been transferred to many institutions and a varity of code version exist throughout academia and industry. One version, rebranded as CTF, is jointly developed and maintained by the Consortium for the Advanced Simulation of LWRs (CASL) and North Carolina State University (NCSU). Since being incorporated into CASL's Virtual Environment for Reactor Applications (VERA), CTF has had rapid improvements relating to its capabilities, parallelism, performance, validation, and quality assurance. This work expands upon existing CASL efforts to further improve the pedigree of CTF.

In order to address the reliability and predictive capability of complex simulation tools, it is necessary to establish a pedigree for these tools. This process is accomplished through a series of tasks, which successively add evidence that a tool is reliable [2, 3, 4].

1. Software Quality Assurance (SQA) is used to minimize code bugs.
2. Code verification ensures that the code is solving the underlying conservation equations correctly.
3. Solution verification quantifies the numerical biases associated with a particular choice of mesh.
4. Validation is used to quantify how well the equations being solved represent reality.
5. Uncertainty Quantification (UQ) attempts to quantify all sources of uncertainty and put bounds on any quantities of interest.

In this work, we address SQA and code verification for the thermal hydraulic subchannel code CTF.

1.1 Verification Matrix

In this work, verification problems are mapped to the conservation equations solved by the code. CTF solves a two fluid, three field formulation of two-phase flow and a conduction equation for the solid.

fluid mass

$$\underbrace{\frac{\partial \alpha\rho}{\partial t}}_{\text{transient}} + \underbrace{\nabla\cdot(\alpha\rho\vec{u})}_{\text{advection}} = \underbrace{\Gamma}_{\text{mass transfer}} + \underbrace{\dot{m}_T}_{\substack{\text{turbulent mixing}\\ \text{void drift}}} \tag{1.1}$$

fluid energy

$$\underbrace{\frac{\partial \alpha\rho h}{\partial t} - \alpha\frac{\partial P}{\partial t}}_{\text{transient}} + \underbrace{\nabla\cdot(\alpha\rho h\vec{u})}_{\text{advection}} = \underbrace{\Gamma h}_{\text{mass transfer}} + \underbrace{q_w}_{\text{convection}} + \underbrace{\dot{h}_T}_{\substack{\text{turbulent mixing}\\ \text{void drift}}} \tag{1.2}$$

fluid momentum

$$\underbrace{\frac{\partial \alpha\rho\vec{u}}{\partial t}}_{\text{transient}} + \underbrace{\nabla\cdot(\alpha\rho\vec{u}\vec{u})}_{\text{advection}} = \underbrace{\alpha\rho g}_{\text{gravity}} - \underbrace{\alpha\nabla P}_{\text{pressure force}} + \underbrace{\tau_w}_{\text{shear}} + \underbrace{\tau_i}_{\text{interfacial shear}} + \underbrace{\tau_T}_{\substack{\text{turbulent mixing}\\ \text{void drift}}} \tag{1.3}$$

solid energy

$$\underbrace{\rho c_p\frac{\partial T}{\partial t}}_{\text{transient}} - \underbrace{\frac{\partial}{\partial x}k\frac{\partial T}{\partial x}}_{\text{conduction}} = \underbrace{Q}_{\substack{\text{internal}\\ \text{generation}}} - \underbrace{q_w}_{\text{convection}} \tag{1.4}$$

Note that the phase indicator has been omitted from the fluid equations, but there are eight equations solved for the fluid fields: three water equations, three steam equations, and two droplet equations. Droplets are assumed to be in thermal equilibrium with water, so there is no energy conservation equation solved for the droplet field. CTF is generally run in subchannel mode, where the advection terms and pressure force are split into an axial and a lateral component. The solid is assumed to have a constant density and does not move, therefore it only has an energy equation.

This work will focus primarily on single-phase liquid verification problems, with a few tests for water-steam mixtures. It is left as a future exercise to implement problems similar to those in this report for the steam, droplet, and noncondesible gas fields. In fact, no existing code verification problems involve either the droplet or noncondensible gas fields.

Given this set of nonlinear coupled partial differential equations, we can formulate the verification matrix. This matrix is shown in Table 1.1. The verification problems are divided into three categories: (1) problems that have already been incorporated into the CTF automated regression suite, (2) problems that are harvested from the literature, and (3) new problems solved in this report. For each chosen verification problem, the involved conservation terms are checked (✓). Many problems involve other terms, though they are not involved in solution of the analytic problem. For example: the CTF steam and droplet fields cannot be disabled, many terms are set very small or very large to approximate the analytic solution, and many terms cancel out due to symmetry. These terms are not checked in the verification matrix since they are essentially removed from the solution.

The verification coverage is relatively good; of all conservation terms, 80% having at least one corresponding

Table 1.1: CTF verification matrix. Only liquid and steam terms are included, as no verification problems involve the droplet or noncondensible gas fields. The tests are split into three categories: those already included in the automated regression suite, those harvested from the literature, and those created for this report. Asterisks (*) indicate problems that were not incorporated into the CTF regression suite due to unsatisfactory results. See the corresponding sections for more details.

		Regression suite					Literature			New tests			
Equation	Term	Heat Exchanger	Turbulent Mixing	Flow Split	Grid Enhancement	Grid Spacer	Isokinetic Advection (2.1)	Linear Conduction (2.2)	Water Faucet* (2.3)	Friction and Gravity (2.4)	Convection (2.5)	Nonlinear Conduction* (2.6)	Pipe Boiling (2.7)
Fluid Mass	transient						✓		✓				
	axial advection						✓		✓				
	lateral advection												
	mass transfer												✓
	turbulent mixing												
Fluid Energy	transient						✓				✓		✓
	axial advection	✓	✓		✓		✓						✓
	lateral advection												
	interfacial transfer												✓
	convection	✓			✓						✓		
	grid enhancement				✓								
	turbulent mixing		✓										
Fluid Momentum	transient								✓				
	axial advection								✓				
	lateral advection								✓				
	gravity			✓					✓	✓			
	axial pressure			✓		✓				✓			
	lateral pressure			✓									
	shear			✓						✓			
	grid enhancement				✓								
	form loss					✓							
	interfacial shear												
	turbulent mixing												
Solid Energy	transient										✓		
	linear conduction							✓					
	nonlinear conduction											✓	
	energy generation							✓				✓	
	convection										✓		
	Two-Phase								✓				✓
	Equation of State					✓	✓		✓				✓

verification test. Mass/momentum turbulent mixing, all three lateral advection terms, and interfacial shear are the only physics with no corresponding tests. These gaps can be filled in the future. Also note that this formulation of the matrix only checks for testing of *individual* terms in the equations. A more thorough method would be to test that all *combinations* of terms are tested, as it is possible that combinations of terms reveal code bugs that are not seen when individual models are tested.

1.2 Formal Order of Accuracy

The formal order of accuracy for each equation can be derived by considering how the chosen discretization schemes behave as the mesh is refined. In this work, all problems have uniform meshes (i.e., Δx and Δt are constant). We demonstrate this process for a one-dimensional single phase mass conservation equation with no sources.

$$\frac{\partial \rho}{\partial t} + \frac{\partial \rho u}{\partial x} = 0 \tag{1.5}$$

This is forward discretized in time and upwinded in space (assuming $u > 0$).

$$\frac{1}{\Delta t}\left(\rho_i^{n+1} - \rho_i^n\right) + \frac{1}{\Delta x}\left(\rho_i^n u_{i+1/2}^{n+1} - \rho_{i-1}^n u_{i-1/2}^{n+1}\right) = 0 \tag{1.6}$$

Here, the superscript is the time index and the subscript is the spatial index. Now, Taylor series expansions about i and n are used to approximate ρ_i^{n+1}, ρ_{i-1}^n, $u_{i+1/2}^{n+1}$, and $u_{i-1/2}^{n+1}$. Only second order terms are included in these approximations.

$$\rho_i^{n+1} = \sum_{k=0}^{\infty} \frac{1}{k!} \left.\frac{\partial^k \rho}{\partial t^k}\right|_i^n \Delta t^k \approx \rho_i^n + \left.\frac{\partial \rho}{\partial t}\right|_i^n \Delta t + \frac{1}{2} \left.\frac{\partial^2 \rho}{\partial t^2}\right|_i^n \Delta t^2 \tag{1.7}$$

$$\rho_{i-1}^n = \sum_{k=0}^{\infty} \frac{1}{k!} \left.\frac{\partial^k \rho}{\partial x^k}\right|_i^n (-\Delta x)^k \approx \rho_i^n - \left.\frac{\partial \rho}{\partial x}\right|_i^n \Delta x + \frac{1}{2} \left.\frac{\partial^2 \rho}{\partial x^2}\right|_i^n \Delta x^2 \tag{1.8}$$

$$\begin{aligned} u_{i+1/2}^{n+1} &= \sum_{k=0}^{\infty}\sum_{m=0}^{\infty} \frac{1}{k!m!} \left.\frac{\partial^{k+m} \rho}{\partial x^k \partial t^m}\right|_i^n \left(\frac{\Delta x}{2}\right)^k \Delta t^m \\ &\approx u_i^n + \frac{1}{2}\left.\frac{\partial u}{\partial x}\right|_i^n \Delta x + \frac{1}{8}\left.\frac{\partial^2 u}{\partial x^2}\right|_i^n \Delta x^2 + \left.\frac{\partial u}{\partial t}\right|_i^n \Delta t + \frac{1}{2}\left.\frac{\partial^2 u}{\partial t^2}\right|_i^n \Delta t^2 + \frac{1}{2}\left.\frac{\partial^2 u}{\partial x \partial t}\right|_i^n \Delta x \Delta t \end{aligned} \tag{1.9}$$

$$\begin{aligned} u_{i-1/2}^{n+1} &= \sum_{k=0}^{\infty}\sum_{m=0}^{\infty} \frac{1}{k!m!} \left.\frac{\partial^{k+m} \rho}{\partial x^k \partial t^m}\right|_i^n \left(-\frac{\Delta x}{2}\right)^k \Delta t^m \\ &\approx u_i^n - \frac{1}{2}\left.\frac{\partial u}{\partial x}\right|_i^n \Delta x + \frac{1}{8}\left.\frac{\partial^2 u}{\partial x^2}\right|_i^n \Delta x^2 + \left.\frac{\partial u}{\partial t}\right|_i^n \Delta t + \frac{1}{2}\left.\frac{\partial^2 u}{\partial t^2}\right|_i^n \Delta t^2 - \frac{1}{2}\left.\frac{\partial^2 u}{\partial x \partial t}\right|_i^n \Delta x \Delta t \end{aligned} \tag{1.10}$$

Now, these Taylor series expansions are incorporated into Equation 1.6, after which the simplified equation becomes (neglecting higher order terms and omitting i and n indices):

$$\frac{\partial \rho}{\partial t} + \frac{\partial \rho u}{\partial x} \approx \left[\frac{u}{2}\frac{\partial^2 \rho}{\partial x^2} + \frac{1}{2}\frac{\partial \rho}{\partial x}\frac{\partial u}{\partial x}\right]\Delta x - \left[\frac{1}{2}\frac{\partial^2 \rho}{\partial t^2} + \frac{\partial u}{\partial t}\frac{\partial \rho}{\partial x} + \rho\frac{\partial^2 u}{\partial x \partial t}\right]\Delta t \tag{1.11}$$

Therefore, the mass equation is first order in both space and time. The same process can be repeated for the energy and momentum equations to show that they are also first order in time and space.

For the solid energy equation, the order of accuracy can easily be derived in one dimension with constant properties.

$$\frac{\partial T}{\partial t} + \alpha\frac{\partial^2 T}{\partial x^2} = 0 \tag{1.12}$$

This is forward-discretized in time and center differenced in space.

$$\frac{1}{\Delta t}\left(T_i^{n+1} - T_i^n\right) + \frac{\alpha}{\Delta x^2}\left(T_{i+1}^{n+1} - 2T_i^{n+1} + T_{i-1}^{n+1}\right) = 0 \tag{1.13}$$

Again, all discrete variables are expanded about the same spatial and temporal location. For this analysis, we use i and $n+1$.

$$T_i^n = \sum_{k=0}^{\infty}\frac{1}{k!}\left.\frac{\partial^k T}{\partial t^k}\right|_i^{n+1}(-\Delta t)^k \approx T_i^{n+1} - \left.\frac{\partial T}{\partial t}\right|_i^{n+1}\Delta t + \frac{1}{2}\left.\frac{\partial^2 T}{\partial t^2}\right|_i^{n}\Delta t^2 \tag{1.14}$$

$$\begin{aligned} T_{i+1}^{n+1} &= \sum_{k=0}^{\infty}\frac{1}{k!}\left.\frac{\partial^k T}{\partial x^k}\right|_i^{n+1}\Delta x^k \\ &\approx T_i^{n+1} + \left.\frac{\partial T}{\partial x}\right|_i^{n+1}\Delta x + \frac{1}{2}\left.\frac{\partial^2 T}{\partial x^2}\right|_i^{n+1}\Delta x^2 + \frac{1}{6}\left.\frac{\partial^3 T}{\partial x^3}\right|_i^{n+1}\Delta x^3 + \frac{1}{24}\left.\frac{\partial^4 T}{\partial x^4}\right|_i^{n+1}\Delta x^4 \end{aligned} \tag{1.15}$$

$$\begin{aligned} T_{i-1}^{n+1} &= \sum_{k=0}^{\infty}\frac{1}{k!}\left.\frac{\partial^k T}{\partial x^k}\right|_i^{n+1}(-\Delta x)^k \\ &\approx T_i^{n+1} - \left.\frac{\partial T}{\partial x}\right|_i^{n+1}\Delta x + \frac{1}{2}\left.\frac{\partial^2 T}{\partial x^2}\right|_i^{n+1}\Delta x^2 - \frac{1}{6}\left.\frac{\partial^3 T}{\partial x^3}\right|_i^{n+1}\Delta x^3 + \frac{1}{24}\left.\frac{\partial^4 T}{\partial x^4}\right|_i^{n+1}\Delta x^4 \end{aligned} \tag{1.16}$$

These Taylor series expansions are incorporated into Equation 1.13, after which the error equation is (neglecting higher order terms and omitting indices):

$$\frac{\partial T}{\partial t} + \alpha\frac{\partial^2 T}{\partial t^2} \approx \frac{1}{2}\frac{\partial^2 T}{\partial t^2}\Delta t - \frac{\alpha}{12}\frac{\partial^4 T}{\partial x^4}\Delta x^2 \tag{1.17}$$

Therefore, the solid energy equation should be second order in space and first order in time. Note that if the assumption of constant properties is relaxed, the analysis is more complex but has the same result.

All expected orders of accuracy are summarized in Table 1.2. Temporal and spatial orders of accuracy are respectively indicated by p_t and p_x. Note that the derivation of these orders can be significantly more complicated (e.g., if there are source terms, nonlinearities, etc.), but these more complex effects are only expected to degrade the order of accuracy if they are implemented incorrectly or cause numerical instabilities.

Table 1.2: Formal order of accuracy for the conservation equations in CTF

Equation	p_x	p_t
Fluid Mass	1	1
Fluid Energy	1	1
Fluid Momentum	1	1
Solid Energy	2	1

Remark. *The formal order of accuracy can be problem-dependent. This happens when the coefficients in the modified equation cancel or are equal to zero. For example, if Equation 1.11 is used to analyze a problem where $\partial\rho/\partial x = 0$, there is no spatial error. If this is the case, the code will predict the analytic solution to within round-off. For an example of this phenomenon, see section 2.4.*

1.3 Verification Procedure

The purpose of verification is to compare the formal and observed orders of accuracy for a particular set of equations and problem. To achieve this, we follow a prescribed process for each of the verification problems.

1. Choose the analytic model to be simulated, the quantities of interest, and formulate the analytic solution.
2. Create a computational CTF model.
3. Ensure that the code output matches relatively well for a base choice of discretization. Significant mismatches at this step can indicate mismatched physics, inconsistent assumptions in the analytic or computed solutions, or errors in the post-processing of code results.
4. Successively refine the computational mesh (in space and/or time) and recompute the CTF quantities of interest.
5. Compute the order of accuracy compared to the analytic solution by calculating the root-mean-square error (RMSE) at each choice of discretization

$$||y|| = \sqrt{\frac{1}{N}\sum_{i=1}^{N}\left(y_{\text{exact}} - y_{\text{computed}}\right)^2}, \tag{1.18}$$

then find the order of accuracy p by fitting a linear line on the log-log plot of error-vs-discretization

$$||y|| = Ch^p \tag{1.19}$$

6. If the observed order of accuracy matches with the formal order (see Table 1.2) to within ± 0.1, the verification procedure is successful. If the observed order is significantly different, the process will require debugging to find the issue. Debugging exercises can include: examination of the Linear Truncation Error (LTE), analysis of spatial and temporal errors, examination of code response, or trying different code options.
7. If the observed order and formal order cannot be matched, a constant error model will be used instead of Equation 1.19:

$$||y|| = C_0 + C_1 h^p \tag{1.20}$$

If the constant error model indicates the correct order of convergence, it indicates that there is a constant error between y_{exact} and y_{computed}. Such cases could indicate a small boundary condition error, small unit conversion errors, small inconsistencies in assumptions between the analytic and computational model, or any number of other issues. If this is the case, we will present the constant error model results. Though there is a constant error, the problem converges numerically with the correct order.

2. Code Verification

The code verification problems in this chapter each fall into one of three categories: (1) already exist in the CTF documentation and regression matrix, (2) are harvested from existing verification work in the literature, or (3) are designed and added in this work. These categories are described in the following paragraphs, then each problem is individually documented throughout the sections in this chapter.

The first category consists of four problems that were added in FY 2019 to address CTF convergence behavior: the heat exchanger, turbulent mixing, flow split, grid enhancement, and a non-convergent grid spacer study. Documentation of each of these can be found in the CTF Verification and Validation Manual [5].

There are three problems that have been documented in the literature but not fully incorporated into CTF: isokinetic advection [6], linear conduction [7], and water faucet [8]. All of these had been incorporated into the testing matrix to some extent, but there were no regression tests that specifically address convergence. As part of this work, the first two of these problems is incorporated into the CTF documentation and regression matrix. The water faucet problem is re-examine, but does not exhibit the expected convergence behavior.

Finally, new problems are designed and analyzed in this report: convection, friction & gravity, nonlinear conduction, and pipe boiling. The first of these tests focuses on transient convective heat transfer between the fluid and solid. The second focuses on the axial pressure drop in a channel. The third addresses temperature-dependent thermal conductivity in a flat plate. The final problem is a two-phase verification test, which is harvested from [9]. All but the nonlinear conduction problem have been added to the CTF regression suite.

2.1 Isokinetic Advection

This section describes a series of three code verification problems that were designed to test the transient and advective terms in the mass and energy equations. These problems were originally applied to CTF in a conference paper [6].

Problem Definition This problem consists of flow through a horizontal pipe with three assumptions: (1) the velocity and pressure are constant, so the momentum equation is redundant, (2) there are no external sources, and (3) the flow remains as single phase water.

Under these conditions, the governing equations of CTF simplify significantly. The momentum equation is eliminated altogether and the mass and energy equations simplify to a temporal and advective component.

$$\frac{\partial \rho}{\partial t} + u\frac{\partial \rho}{\partial x} = 0 \tag{2.1}$$

$$\frac{\partial \rho h}{\partial t} + u\frac{\partial \rho h}{\partial x} = 0 \tag{2.2}$$

The analytic solution to this problem is simply the advection of the inlet condition with the velocity u. Three different inlet conditions are chosen to test the advection of various wave shapes: (1) a discontinuous square wave, (2) a cosine wave, and (3) a hyperbolic tangent. The respective analytic solution for each of these inlet conditions are shown here [6].

$$\gamma_{sq} = \begin{cases} \gamma_o, & ut \leq x \\ \gamma_{in}, & ut > x \end{cases} \tag{2.3}$$

$$\gamma_{tanh} = \begin{cases} \gamma_o, & ut \leq x \\ \frac{1}{2}\left[(\gamma_o + \gamma_{in}) - (\gamma_o - \gamma_{in})\tanh\left(\frac{u(t-\tau)-x}{l}\right)\right], & ut > x \end{cases} \tag{2.4}$$

$$\gamma_{cos} = \begin{cases} \gamma_o, & ut \leq x \\ \frac{1}{2}\left[(\gamma_o + \gamma_{in}) + (\gamma_o - \gamma_{in})\cos\left(\frac{2\pi}{p}\left(t - \frac{x}{u}\right)\right)\right], & ut > x \end{cases} \tag{2.5}$$

Here, γ can be either density ρ or enthalpy h. All necessary parameters are defined in Table 2.1. The initial and inlet quantities were iteratively selected such that the velocity and pressure are approximately constant. Note that the inlet boundary conditions listed in the table fully define the time-dependent inlet conditions.

CTF Input The CTF input consists of a single channel with standard boundary conditions. The square wave and cosine wave are run for five seconds, the hyperbolic tangent is run for ten. To maintain consistency with the assumptions of this problem, a few simplifications to the input deck are necessary.

- There is an approximately constant pressure throughout the domain. This could be achieved by fixing the density and advecting an energy wave; however, this problem employs both the energy and density advection terms. To achieve this while using a real equation of state, density and enthalpy differences are set such that they have approximately equal and opposite effects on pressure.
- The variation in density and enthalpy through the wave remains small, which maintains an approximately constant velocity.

Table 2.1: Parameters for isokinetic advection verification problems

Type	Parameter	Symbol	Value
Geometry	Channel length	L	0.5 m
	Flow area	A	0.0001 m^2
	Wetted perimeter	P_w	0.040 m
Boundary condition	Outlet pressure	P	1 bar
	Inlet flow rate	$\dot{m}_{in}$	0.050 04 kg/s
	Inlet enthalpy	h_{in}	159.22 kJ/kg
	Hyperbolic tangent width	l	0.05 m
	Hyperbolic tangent offset	τ	5.0 s
	Cosine wave period	p	L/u
Initial condition	Initial flow rate	$\dot{m}_o$	0.005 kg/s
	Initial enthalpy	h_o	167.6 kJ/kg

- All source terms are set to zero using exposed parameters for Verification, Validation, and Uncertainty Quantification (VVUQ) studies. This includes turning off friction and gravity, which removes any expected pressure drops.

The simulation is transient and both Δt and Δx are refined at the same rate during the verification study. This way, the Courant-Friedrichs-Lewy (CFL) limit ($u\Delta t/\Delta x$) is constant, which precludes numerical instabilities for the CTF discretization scheme.

Results Under the conditions described thus far in this section, the expected behavior with diffusive error is demonstrated for both temporal and spatial convergence. The problems presented in this section are incorporated into the CTF regression suite.

The results for a square, cosine, and hyperbolic tangent waves are shown respectively in Figures 2.1, 2.2, and 2.3. For each wave type, three plots are included. First, the solution for various choices of meshing is shown against the analytic solution at the final simulation time. Second, the corresponding point-wise errors are plotted. Finally, the convergence of the error is demonstrated.

For the cosine and hyperbolic tangent waves, the convergence study is first order (respectively $p \approx 0.925$ and $p \approx 0.937$). For the square wave, the order of convergence is degraded by the discontinuity being advected, so the problem is convergent but with sub-unity convergence ($p \approx 0.204$). This sub-linear convergence behavior is described in more detail in [10], where the expected behavior for constant CFL refinement is $p = 0.25$.

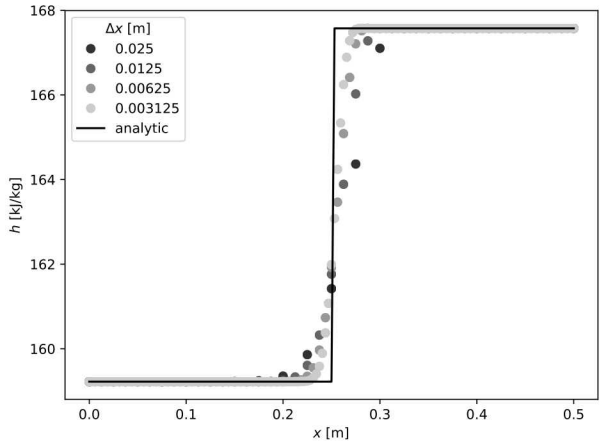

(a) Enthalpy at $t = 5\,\mathrm{s}$

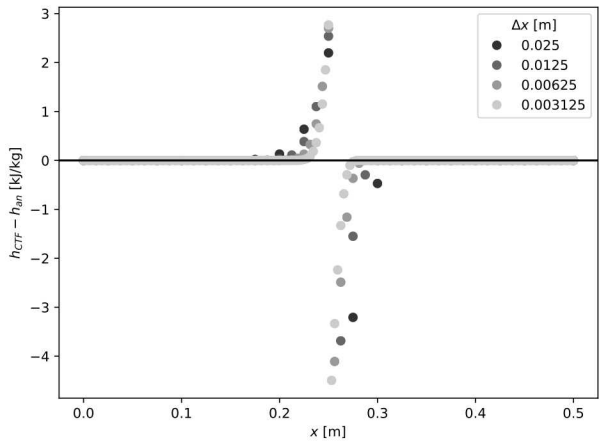

(b) Error in enthalpy at $t = 5\,\mathrm{s}$

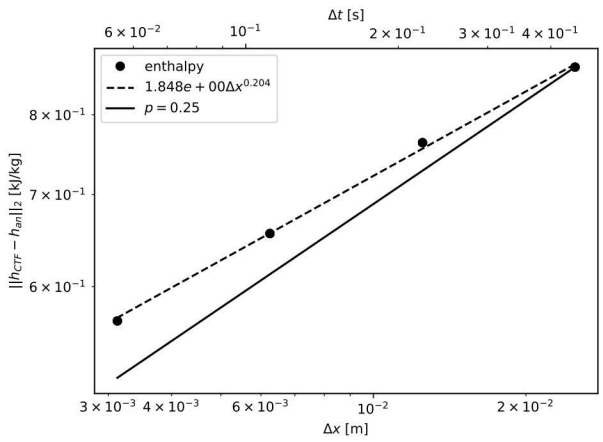

(c) Convergence plot

Figure 2.1: Results for the isokinetic advection verification problem using a square wave

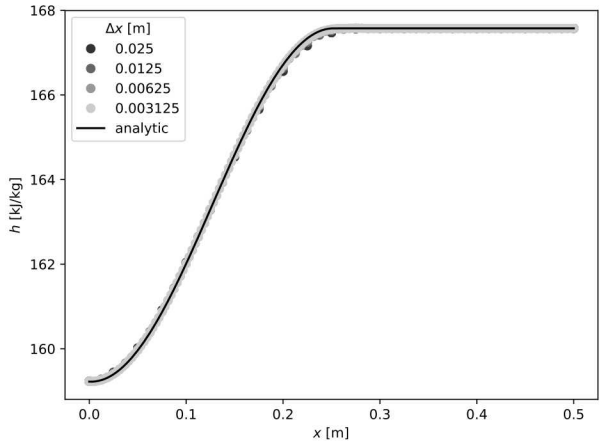

(a) Enthalpy at $t = 5\,\mathrm{s}$

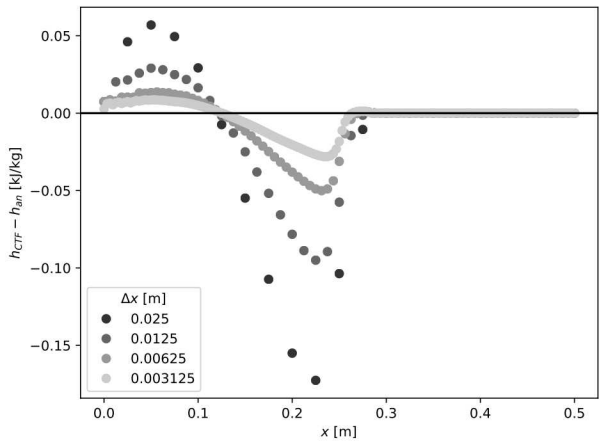

(b) Error in enthalpy at $t = 5\,\mathrm{s}$

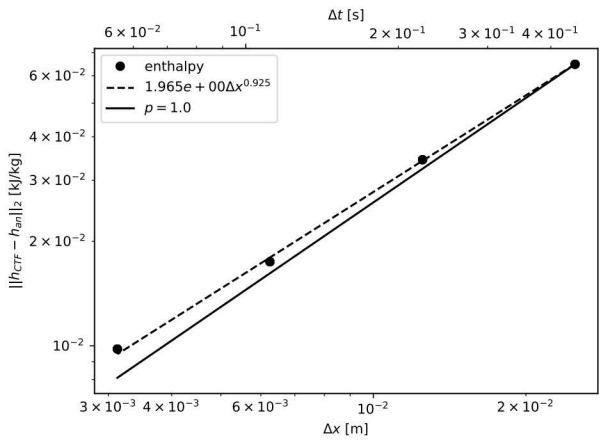

(c) Convergence plot

Figure 2.2: Results for the isokinetic advection verification problem using a cosine wave

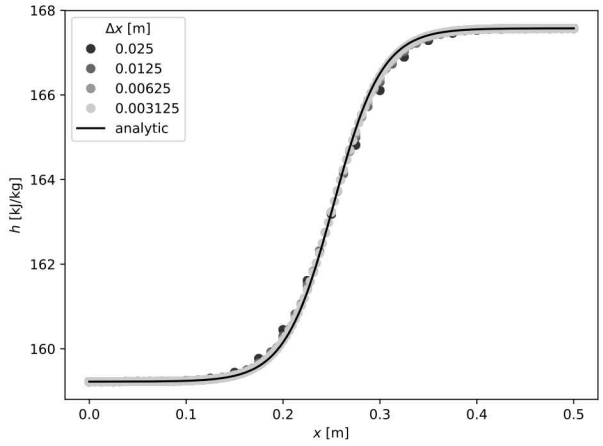

(a) Enthalpy at $t = 5\,\mathrm{s}$

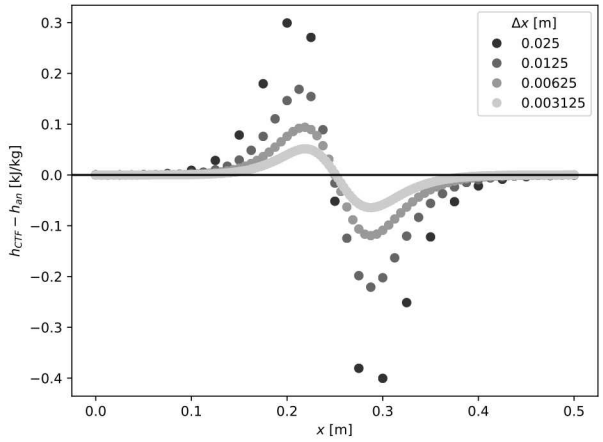

(b) Error in enthalpy at $t = 5\,\mathrm{s}$

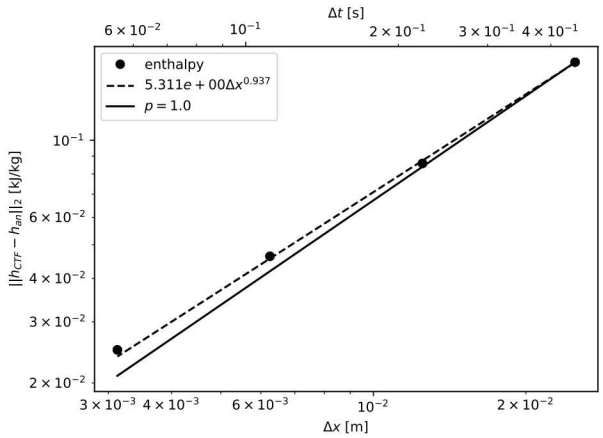

(c) Convergence plot

Figure 2.3: Results for the isokinetic advection verification problem using a hyperbolic tangent wave

2.2 Linear Conduction

In this section, the temperature distribution in a solid cylinder is verified to converge to the analytic solution at the correct rate. This study is a modification of the verification work performed in [7].

Problem Definition The conduction equation in CTF is

$$\rho c_p \frac{\partial T}{\partial t} - \nabla \cdot (k \nabla T) + q''' = 0. \tag{2.6}$$

This equation is significantly simplified: (1) only the steady state temperature distribution is found, (2) it is solved for one-dimensional radial conduction in radial coordinates, (3) all solid properties are constant, and (4) internal heat generation is constant. Under these conditions, the conservation equation is

$$\frac{k}{r}\frac{d}{dr}\left(r\frac{dT}{dr}\right) + q''' = 0. \tag{2.7}$$

In cylindrical geometry with a surface temperature boundary condition $T(r = r_f) = T_f$, the solution to the posed equation is

$$T(r) = T_f + \frac{q'}{4\pi k_f}\left(1 - \frac{r^2}{r_f^2}\right). \tag{2.8}$$

For a nuclear fuel rod, the cladding and gap are also included in the geometry, so these must be accounted for in the analytic solution. Therefore, the additional temperature drop between the fuel surface (r_f) and the outer cladding surface is added to the boundary condition in the analytic solution.

$$T_f - T_{co} = \frac{q'}{2\pi r_f h_{gap}} + \frac{q'}{2\pi k_c}\ln\left(\frac{r_{co}}{r_{ci}}\right) \tag{2.9}$$

Remark. *The cladding and gap mesh is fixed in CTF, and therefore a constant spatial error is added between the pin surface temperature and the rode surface temperature. The analytic solution to Equation 2.9 is* $T_f - T_{co} \approx 538.4\,\mathrm{K}$. *However, the CTF computed temperature difference over this region is* $T_f - T_{co} \approx 537.3$. *When the analytical solution is calculated in the verification script, it uses the computed temperature increase to set the boundary condition* $T(r_f) = T_f$. *In this way, the numerical error introduced by the gap and clad disretization is minimized, and we are only concerned with the numerical uncertainty in the fuel rod discretiztion.*

All variables required to find the analytic solution are defined in Table 2.2. This includes geometry, all properties, the boundary conditions, and the linear heat rate.

Table 2.2: Parameters for linear conduction verification problem

Type	Parameter	Symbol	Value
Geometry	Fuel surface radius	r_f	0.5430 cm
	Clad inside radius	r_{ci}	0.6370 cm
	Clad outside radius	r_{co}	0.6402 cm
Solid property	Fuel conductivity	k_f	7 W/m/K
	Clad conductivity	k_c	7 W/m/K
	Gap conductance	h_g	1000 W/m^2/K
Boundary condition	Clad outside temperature	T_{co}	300 K
Source terms	Linear heat rate	q'	18.3 kW/m

CTF Input The CTF input is created using CTF's stand-alone fuel solver, CTFFuel [7]. All input configuration is straight-forward. The cladding and gap discretization is fixed in CTF, therefore only the temperature distribution inside the fuel pellet is plotted and analyzed for convergence. For the verification study, all inputs are identical for successive simulations except for the number of radial rings in the fuel region.

Results The results for the linear conduction problem are shown in Figure 2.4. The temperature distribution in the fuel pin predicted by CTF matches very closely with the analytic solution. The center of the cylinder is furthest from the surface boundary condition and therefore exhibits an accumulation of the spatial error. As the discretization is refined, this concentration of error at the center of the cylinder rapidly decreases. As defined in section 1.2, the formal order of accuracy for spatial error in this equation is second order. The convergence plot shows an observed order very close to this, $p = 1.987$.

2.3 Water Faucet

This section describes the first two-phase code verification problem performed in CTF. This problem is a quintessential verification problem for one-dimensional six equation two-phase flow [9]. Verification using this problem was originally performed in [8], but only a single mesh was included in the regression testing suite.

Problem Definition Initially, a pipe with uniform cross-sectional area is filled with a uniform column of liquid moving at a constant velocity. An annulus of gas surrounds the liquid and is stationary. Starting at some initiating time, gravity causes the liquid column to accelerate downwards and the water column becomes thinner over time.

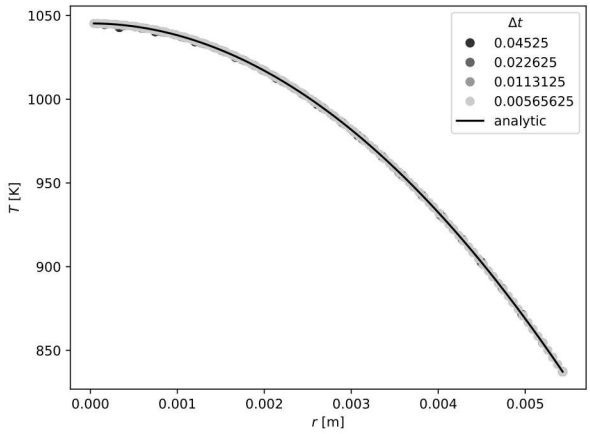

(a) Steady state temperature distribution

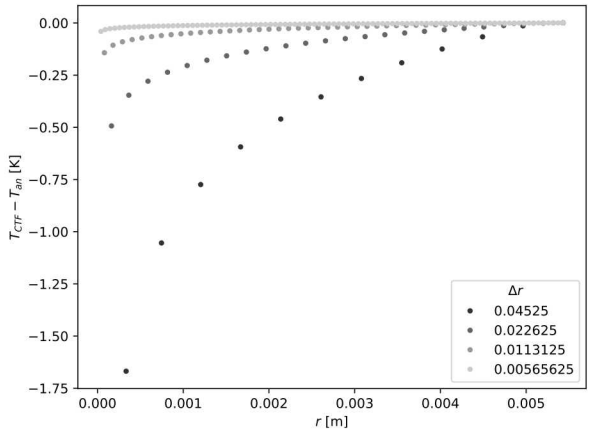

(b) Error in steady state temperature

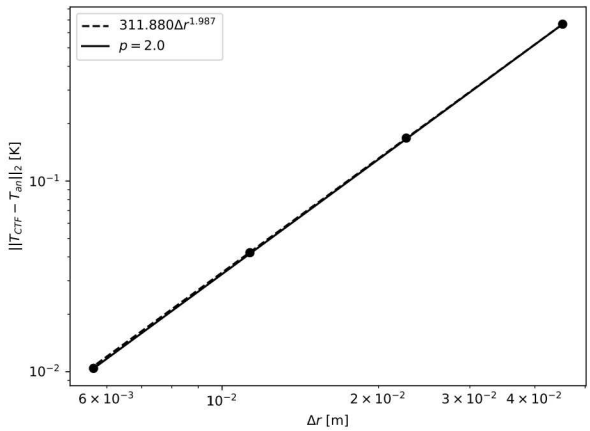

(c) Convergence plot

Figure 2.4: Results for linear conduction verification problem

The six-equation model used for this analytic solution can be summarized by the mass, momentum, and energy equation for each phase. We assume no interfacial transfer and no wall friction.

$$\frac{\partial \alpha_k \rho_k}{\partial t} + \frac{\partial \alpha_k \rho_k u_k}{\partial x} = 0 \tag{2.10}$$

$$\frac{\partial \alpha_k \rho_k u_k}{\partial t} + \frac{\partial \alpha_k \rho_k u_k^2}{\partial x} + \frac{\partial P}{\partial x} - \alpha_k \rho_k g = 0 \tag{2.11}$$

$$\frac{\partial \alpha_k \rho_k E}{\partial t} + \frac{\partial \alpha_k \rho_k u_k E_k}{\partial x} + \frac{\partial \alpha_k u_k P}{\partial x} = 0 \tag{2.12}$$

Here, k indicates either the fluid or vapor phase. Significant simplifications to this equation set are made for this problem: (1) the problem is isothermal and therefore the energy equations are omitted, (2) the vapor mass is negligible, (3) the pressure variations in the liquid phase are negligible, and (4) both fields have a constant density. Under these simplifications, the governing equations become:

$$\frac{\partial \alpha_l}{\partial t} + \frac{\partial \alpha_l u_l}{\partial x} = 0 \tag{2.13}$$

$$\frac{\partial \alpha_l u_l}{\partial t} + u_l \frac{\partial u_l}{\partial x} - g = 0 \tag{2.14}$$

The solution to this set of equations with initial conditions $\alpha(t=0) = \alpha_0$, $u_l(t=0) = u_0$ and boundary conditions $\alpha(x=0) = \alpha_0$, $u_l(x=0) = v_0$ is outlined in [11].

$$\alpha = \begin{cases} 1 - \frac{(1-\alpha_0)u_0}{\sqrt{u_0^2+2gx}}, & \text{if } x \leq x_d \\ \alpha_0, & \text{if } x > x_d \end{cases} \tag{2.15}$$

$$u_l = \begin{cases} \sqrt{u_0^2 + 2gx}, & \text{if } x \leq x_d \\ u_0 + gt, & \text{if } x > x_d \end{cases} \tag{2.16}$$

Here, the location of the void fraction discontinuity is defined as $x_d = u_0 t + gt^2/2$. Recently, new solutions to this problem have been proposed which relax the massless gas phase assumption [12]. However, the original solutions are sufficiently accurate for low pressures, where $\rho_l/\rho_g >> 1$. All necessary conditions for this problem are defined in Table 2.3.

CTF Input Original implementation of this problem required significant changes to the CTF source code [8]. First, an interfacial pressure correction term was added to the momentum equation.

$$S_{IPC} = \delta \frac{\alpha_v \alpha_l \rho_v \rho_l}{\alpha_v \rho_v + \alpha_l \rho_l} (u_v - u_l)^2 \frac{\partial \alpha_k}{\partial x} \tag{2.17}$$

Table 2.3: Parameters for water faucet verification problem

Type	Parameter	Symbol	Value
Geometry	Pipe length	L	12 m
	Flow area	A_f	0.785 m^2
BC/IC	Void fraction	α_0	0.2
	Liquid velocity	v_0	10 m/s
	Outlet pressure	P	10 bar

Here, δ is a multiplier which turns the correction term on and off. The interfacial pressure correction term can be derived from purely mathematical considerations to eliminate negative eigenvalues in the incompressible limit [13, 14]. In addition, it was necessary to implement a void fraction boundary condition at the channel outlet.

Results The results for the water faucet problem are shown in Figure 2.5. Overall, the CTF solution does seem to be converging to the analytical solution. However, these results are not consistent with the results in [8]. There is anomalous behavior at the inlet of the pipe; it appears that the boundary conditions are not being properly applied at the inlet. Therefore, a meshing-dependent error is introduced to the problem. Due to this bias, the CTF solution is not first order. Therefore, these results are not included in the CTF automated regression suite. It is left as future work to troubleshoot these results and identify the discrepancy with [8].

Remark. *A change implemented by Delchini in [8] was reverted in* `Chan_type.f90` *involving the* `k_init_sol_with_bc` *VUQ multiplier. Re-enabling this change removes some of the oscillations from Figure 2.5, but does not result in a first-order solution. The inlet boundary problem still exists. Additionally, these results were reproduced at various historical points during the implementation of the interfacial pressure correction term (using Github commits). No significant changes to the results were found.*

2.4 Friction and Gravity

In this section, we verify the pressure distribution in CTF, focusing on the friction and gravity components. Various defect tests have been performed focusing on the axial pressure distribution as well as a solution verification study [15]. However, no code convergence study focusing on these phenomena has been performed as of yet.

Problem Description Single phase flow with constant properties passes through a vertical tube. The pressure is fixed at the tube outlet. At steady state, the inlet pressure is larger than the outlet pressure due

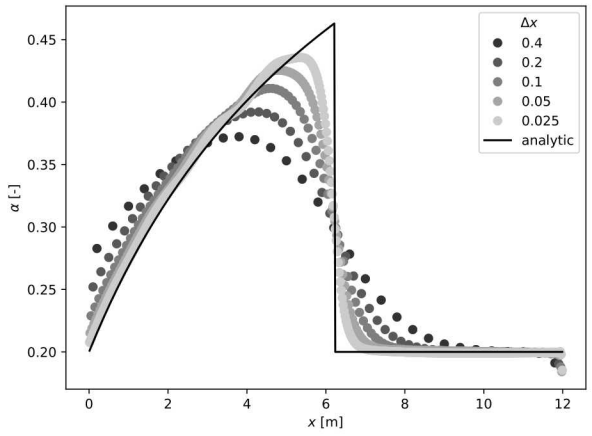

(a) Distribution of void fraction

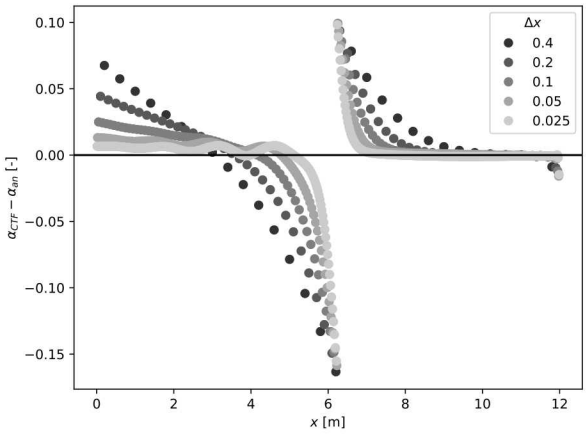

(b) Error in void fraction

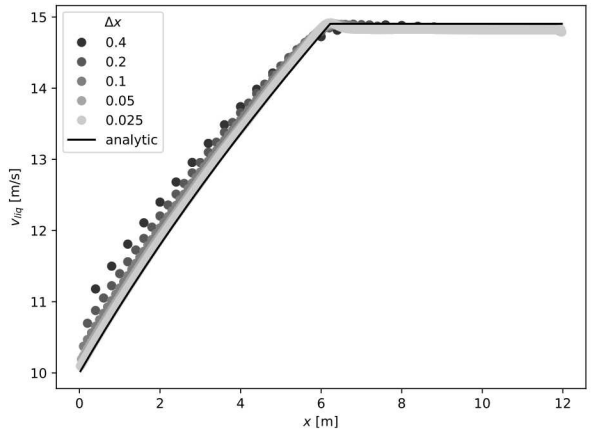

(c) Distribution of liquid velocity

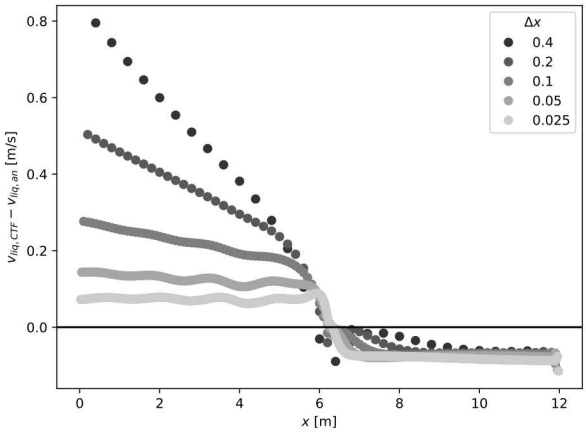

(d) Error in liquid velocity

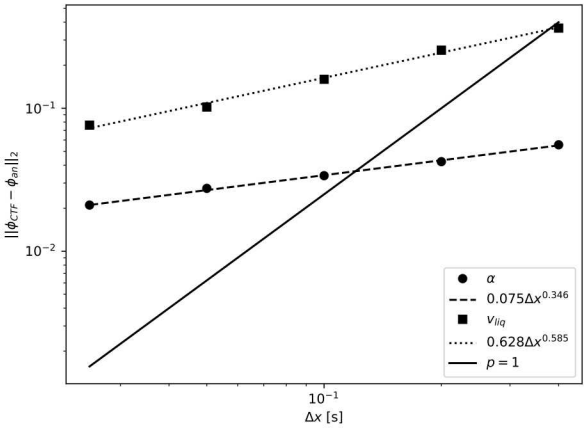

(e) Convergence plot

Figure 2.5: Results for the water faucet verification problem

to gravitational and frictional heads.

We make the following assumptions: (1) steady state and one-dimensional flow, (2) constant density and velocity, (3) pipe geometry with a constant cross-section, (4) constant friction factor, and (5) isothermal flow. Under these conditions, the mass and energy equation are eliminated and the momentum equation is

$$\frac{\partial P}{\partial x} - \rho g = f\frac{\rho u^2}{2D}. \tag{2.18}$$

The equation is integrated and an outlet boundary condition $P(L) = P_{out}$ is applied. In this case, the analytic solution becomes

$$P(x) = P_{out} - \left[f\frac{\rho u^2}{2D_h} + \rho g\right](L - z). \tag{2.19}$$

All parameters necessary to define the problem are listed in Table 2.4.

Table 2.4: Parameters for friction and gravity verification problem

Type	Parameter	Symbol	Value
Geometry	Pipe diameter	D	0.01 m
	Pipe length	L	1 m
Fluid property	Density	ρ	1000 kg/m^3
Boundary condition	Inlet mass flow	$\dot{m}_{in}$	0.1 kg/s
	Outlet pressure	P_{out}	150 bar
Source term	Gravity	g	9.814 56 m/s^2
	Friction factor	f	0.002

Remark. *The value for gravitational constant g is calculated by converting the value used in CTF (`GC` is defined as 32.2 ft/s^2) to SI units.*

CTF Input The CTF input is created as a single channel with geometry consistent with Table 2.4. Inlet mass flow, inlet enthalpy, and outlet pressure are fixed. The simulation is run for one second, after which it has reached steady state. The pressure distribution is extracted and compared to Equation 2.19.

Results The results are shown in Figure 2.6. First, we note that the pressure distribution is very accurately calculated in CTF. In this problem, the pressure drop is a linear function of axial location; therefore, all sources of LTE cancel in the momentum equation (since $\partial^2 P/\partial x^2 = 0$). Therefore, the formal order of accuracy for this particular problem is $p = 0$. CTF should exactly predict the pressure distribution to within round-off. However, there is a bias of about 8 Pa (8×10^{-5} bar) in the total pressure drop. This is a very small—and likely acceptable—bias.

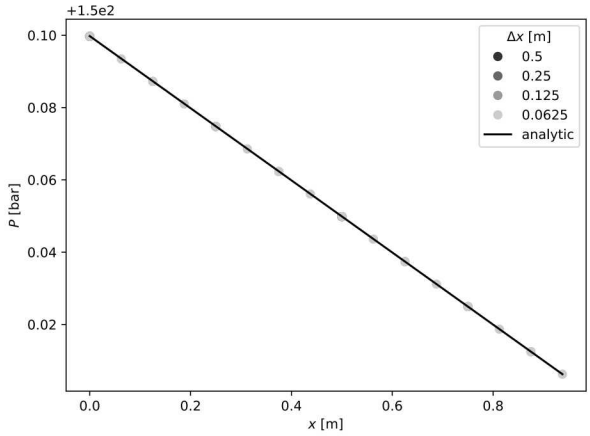

(a) Pressure

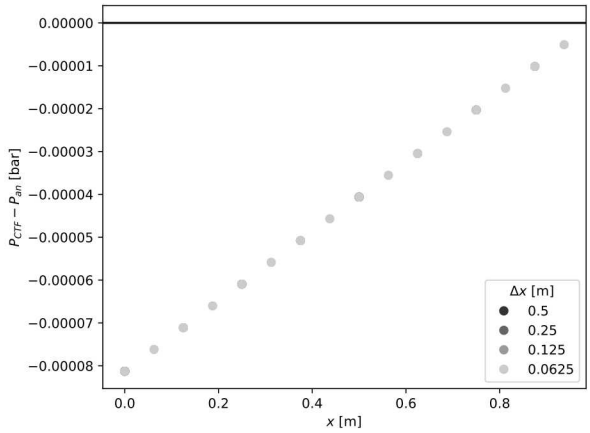

(b) Error

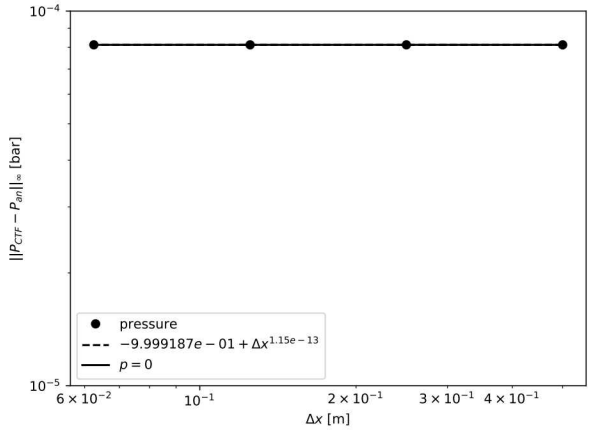

(c) Error convergence

Figure 2.6: Results for friction with gravity verification problem

2.5 Convection

In this problem, heat transfer takes place between a solid and a stationary single phase fluid. This problem is designed specifically to test wall heat transfer (i.e., convection), which governs the energy coupling between the solid and fluid solutions.

Problem Description We make the following assumptions: (1) the fluid and solid can be represented as zero-dimensional control volumes, (2) the fluid and solid are both stationary, (3) all properties are constant, (4) the heat transfer coefficient is constant, and (5) there is no heat generation. Under these conditions, the coupled ordinary differential equations to be solved are

$$V_f \rho_f c_{pf} \frac{\partial T_f}{\partial t} = hA(T_s - T_f) \tag{2.20}$$

$$V_s \rho_s c_{ps} \frac{\partial T_s}{\partial t} = -hA(T_s - T_f). \tag{2.21}$$

If the initial conditions $T_f(0) = T_{f0}$ and $T_w(0) = T_{w0}$ are applied, the solutions for T_f and T_w can be found as a function of time. To simplify the analytic solution, we define the thermal capacitance of the k field as $C_k = V_k \rho_k c_{pk}$.

$$T_f = \frac{1}{C_f + C_s}\left[C_f T_{f0} + C_s T_{s0} + (T_{f0} - T_{s0})\, C_s \exp\left(-\frac{hA(C_f + C_s)}{C_f C_s} t\right)\right] \tag{2.22}$$

$$T_s = \frac{1}{C_f + C_s}\left[C_f T_{f0} + C_s T_{s0} - (T_{f0} - T_{s0})\, C_f \exp\left(-\frac{hA(C_f + C_s)}{C_f C_s} t\right)\right] \tag{2.23}$$

The parameters for this problem are defined in Table 2.5. Note that all quantities in Equations 2.22 and 2.23 can be derived from the parameters in the table. For example, the heat transfer coefficient is related to the Nusselt number via $Nu = hD/k_f$.

CTF Input The CTF input deck for this problem required many iterations before the simulation results matched with the analytic solution. It required that the following simplifications are made:

1. Fluid properties are fixed using the `thermophysical_properties.dat` file and solid properties are fixed using CTF input card group 10.
2. All external sources are disabled using the `vuq_mult.txt` file and the Nusselt number is fixed using `vuq_param.txt`.
3. To properly fix the Nusselt number, underrelaxation of the heat trasfer coefficient must be disabled. This is done in the newly created input card 1.5.
4. The flow rate must be initialized slightly greater than zero so that $Re \neq 0$, as $Nu = 0$ under this particular condition. This is achieved by initializing the fluid flow rate to 1×10^{-100} kg/s.

Table 2.5: Parameters for convection verification problem

Parameter	Symbol	Value	
Geometry	Control volume height	Δx	0.1 m
	Flow area	A_f	0.0001 m^2
	Wetted perimeter	P_w	0.04 m
	Rod diameter	D_r	0.05 m
	Surface area	A	3.142×10^{-3} m^2
Properties	Fluid density	ρ_f	900 kg/m^3
	Solid density	ρ_s	900 kg/m^3
	Fluid specific heat	c_{pf}	4.25 kJ/kg/°C
	Solid specific heat	c_{ps}	4.25 kJ/kg/°C
	Fluid thermal conductivity	k_f	1 W/m/°C
Initial conditions	Initial fluid temperature	T_{f0}	140 °C
	Initial solid temperature	T_{s0}	160 °C
Source terms	Nusselt number	Nu	10

5. The fluid control volume is isolated from the surrounding ghost cells using an approximately zero-flow boundary at the inlet. Because fluid properties are fixed, the conservation of mass dictates that there is also zero-flow at the outlet.
6. CTF does not allow a solid to be defined as a single control volume. Therefore, two control volumes are used and the surface volume is isolated from the center volume by making thermal conductivity very small ($k \approx 0$).

Results The results are shown in Figure 2.7. The thermal capacitance of the solid is larger than the fluid, so the fluid temperature changes more over the transient. The point-wise error is shown and all spatial points appear to display first order convergence. The error between the code solution and analytic solution converges at approximately $p = 1.06$ for both the solid and fluid solution. Therefore, the code displays the expected first order convergence for the solid-to-liquid coupling.

2.6 Nonlinear Conduction

If thermal conductivity is temperature-dependent, the solid energy equation becomes nonlinear and difficult to solve. Usually, these problems are solved numerically, but analytic solutions are possible for a few simple cases. In this section, it is verified that the averaging of thermal conductivity to cell faces does not degrade the order of accuracy of the conduction solution.

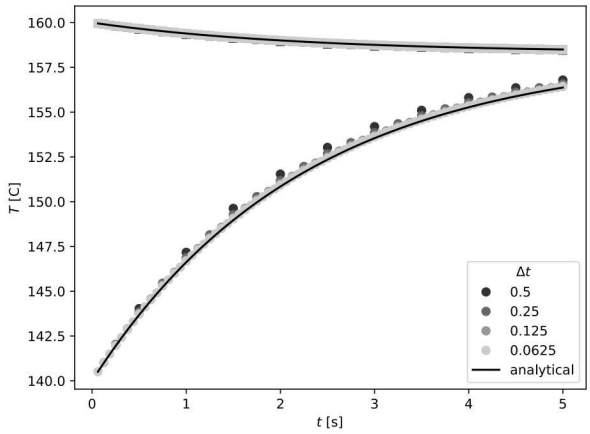

(a) Temperature

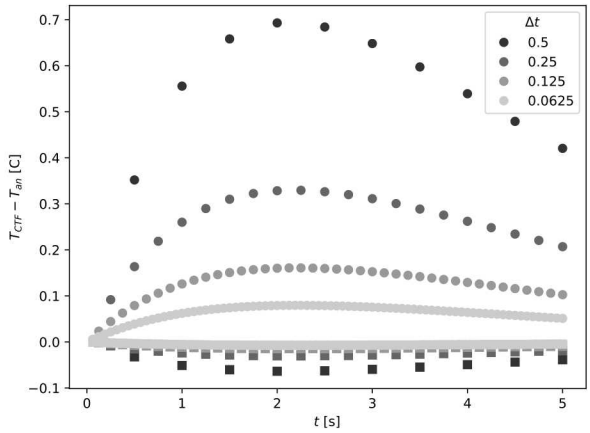

(b) Error

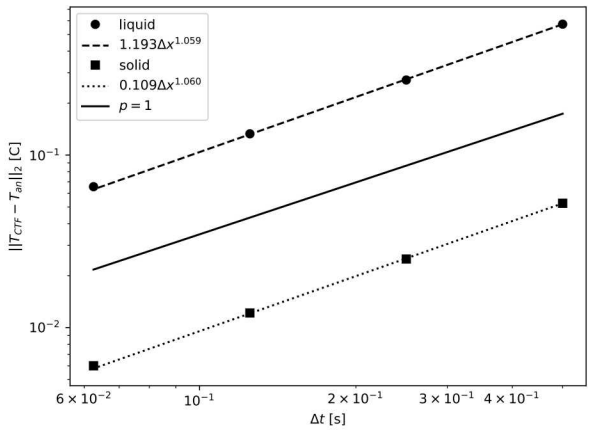

(c) Error convergence

Figure 2.7: Results for the convection verification problem

Problem Description We make the following assumptions: (1) steady state solution, (2) one dimensional Cartesian conduction, (3) all properties and geometry are constant except for thermal conductivity, and (4) there is no internal heat generation. Under these conditions, the conservation equation to be solved is

$$\frac{d}{dx}\left(k(x)\frac{dT}{dx}\right) = 0 \tag{2.24}$$

The boundary conditions are $T(x = 0) = T_0$ and $T(x = L) = T_L$. The thermal conductivity is a linear function of temperature $k = k_L + \beta\,(T - T_L)$, where $k(T_0) = k_0$ and $k(T_L) = k_L$. The solution to this problem is [16]

$$T(x) = T_L + \left[\frac{k_L}{\beta}\sqrt{1 + \beta\frac{k_0 + k_L}{k_L^2}\frac{L - x}{L}\,(T_0 - T_L)} - 1\right]. \tag{2.25}$$

The parameters defining this problem are outlined in Table 2.6.

Table 2.6: Parameters for the nonlinear conduction problem

Parameter	Symbol	Value
Wall thickness	L	0.01 m
Left boundary condition	T_0	155 °C
Right boundary condition	T_L	150 °C
Right thermal conductivity	k_L	5 W/m/°C
Thermal conductivity slope	β	2 W/m

CTF Input For this problem, we create an unheated wall connected on each side to a channel. Each channel has a large flow rate with constant temperature inlet condition, and the heat transfer coefficient to the wall is very large. This approximates a constant temperature boundary condition. The linear function of thermal conductivity is defined using a table in card group 10.

Remark. *CTF infrastructure does not allow a suitable version of this problem to be simulated, so it is not added to the automated regression suite. This is because:*

- *CTF does not print the temperature distribution inside unheated conductors in any of its output files (text, VTK, or HDF5),*
- *A CTF heated conductor cannot be used to simulate wall geometry,*
- *An analytic solution for this problem exists for tube geometry, but a CTF heated tube cannot have boundary conditions defined simultaneously on its inside and outside surfaces, and*
- *CTFFuel is restricted to solving nuclear fuel geometry.*

In this paper, we present promising results (output was extracted directly using hard-coded Fortran `write` *statements) and leave it as a future exercise to add this problem to the regression suite after relaxing one or more of the above restrictions.*

Results The results are shown in Figure 2.8. CTF does seem to approximate the temperature distribution in the wall. The computational solution monotonically converges to the analytic solution; however, the observed order is too far from the formal order to conclude that this problem is free of code bugs. Further analysis will be necessary and this problem is not included in the automated testing suite.

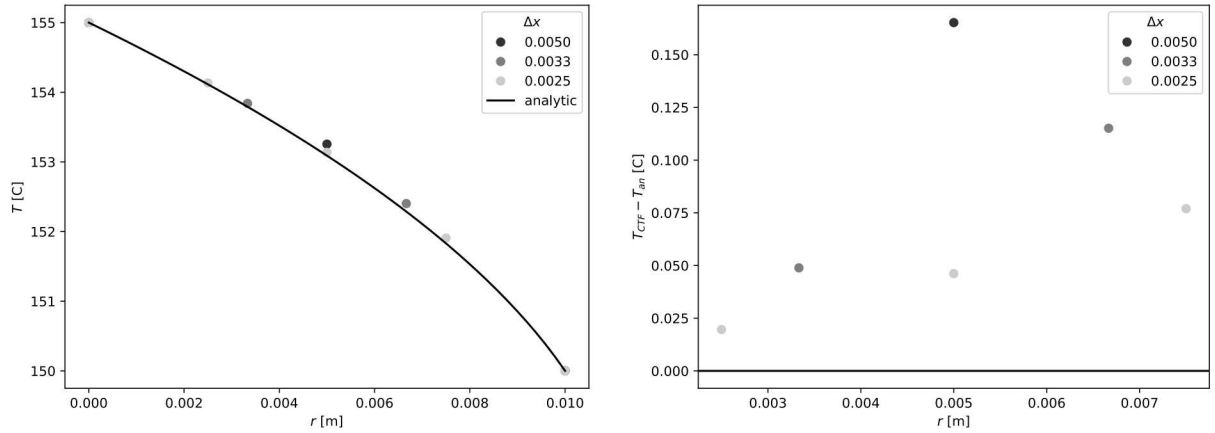

(a) Temperature

(b) Error

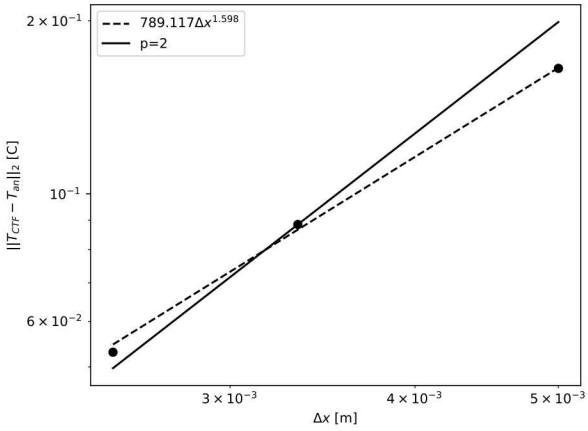

(c) Error convergence

Figure 2.8: Results for the nonlinear conduction verification problem

2.7 Pipe Boiling

In this problem, we verify that interfacial transfer properly conserves energy and doesn't degrade the expected order of accuracy.

Problem Description Saturated water flows through a pipe and a specified amount of heat is added directly to the fluid. The water is initially saturated, so all energy is added as latent heat, which increases the amount of steam.

First, we make the following assumptions which allow the CTF energy equations to be approximated using mixture equations: (1) there is not a significant amount of droplets, and (2) the liquid and steam are in mechanical and thermal equilibrium. Under these conditions, we solve the mixture energy equation.

$$\frac{\partial \rho_m h_m}{\partial t} + \frac{\partial \rho_m u_m h_m}{\partial x} = \dot{q} + \alpha \frac{\partial P}{\partial t} \tag{2.26}$$

The following assumptions further simplify the mixture equation: (1) the heat flux is small enough that P, ρ_m, and u_m are constant throughout the domain, (2) the heat flux is constant in time and has a cosine shape in space.

$$\rho_m \frac{\partial h_m}{\partial t} + \rho_m u_m \frac{\partial h_m}{\partial x} = \frac{q'_o}{A_f} \sin\left(\pi \frac{x}{L}\right) \tag{2.27}$$

The inlet energy boundary condition is set such that the flow is fully saturated water: $h(x = 0) = h_o$. The initial condition sets the entire domain to the same enthalpy: $h(t = 0) = h_o$. Under these conditions, the analytic solution for enthalpy as a function of time and space can be found.

$$h(x,t) = h_o + \frac{q'_o L}{\dot{m}\pi}\left[\cos\left(\pi \frac{ut - x}{L}\right) - \cos\left(\pi \frac{x}{L}\right) + 2H\left[ut - x\right] \sin^2\left(\pi \frac{ut - x}{2L}\right)\right] \tag{2.28}$$

Here, $H[\phi]$ indicates a heavyside function:

$$H[\phi] = \begin{cases} 0, & \phi < 0 \\ 1, & \phi > 0 \end{cases} \tag{2.29}$$

All parameters necessary to fully define this problem are shown in Table 2.7. Note that the inlet/initial enthalpy are calculated using a direct call to CTF property tables.

Table 2.7: Parameters for pipe boiling verification problem

Type	Parameter	Symbol	Value
Geometry	Flow area	A	$0.0001\,\mathrm{m}^2$
	Pipe length	L	$1\,\mathrm{m}$
Boundary condition	Inlet mass flow	$\dot{m}_{in}$	$0.1\,\mathrm{kg/s}$
	Inlet enthalpy	h_o	$1630.554\,\mathrm{kJ/kg}$
	Outlet pressure	P_{out}	$155\,\mathrm{bar}$
Initial condition	Initial enthalpy	h_o	$1630.554\,\mathrm{kJ/kg}$
Source term	Maximum heat rate	q'_o	$10\,\mathrm{kW/m}$

CTF Input There are four details which should be discussed about the modeling of this problem in CTF

1. The wall heat flux is deposited directly into the fluid using the `DHFRAC` input in CTF card 1.2. This bypasses the conduction solution and calculation of the heat transfer coefficient.
2. The cosine shape of the wall heat flux is achieved using a table in Card 11.4. It has 13 digits of accuracy and is defined at each grid location used in the verification study.
3. Wall friction is disabled using `vuq_param.txt` and gravity is disabled using `vuq_mult.txt`.
4. Interfacial friction is many orders of magnitude larger than usual, which approximates mechanical equilibrium between the two phases.

Even so, the analytic solution uses Homogeneous Equilibrium Model (HEM) assumptions to find the enthalpy distribution in the pipe. This is not quite equivalent to the CTF two-fluid model used for this problem. Therefore, we expect a small bias caused by these model mismatches.

Results The CTF results are shown in Figure 2.9. The enthalpy distribution at $t = 0.2\,\mathrm{s}$ is shown for different choices of mesh. It appears that the solution is approaching the analytic solution, but with a small bias. This is confirmed in the convergence plot, which indicates that the CTF solution is approaching a constant error as the mesh is refined. To account for this in the calculation of the observed order of accuracy, a constant error model is used: $\varepsilon = \varepsilon_o + ch^p$. Using this error model, the order of accuracy is approximately $p = 0.96$, which is sufficiently close to one.

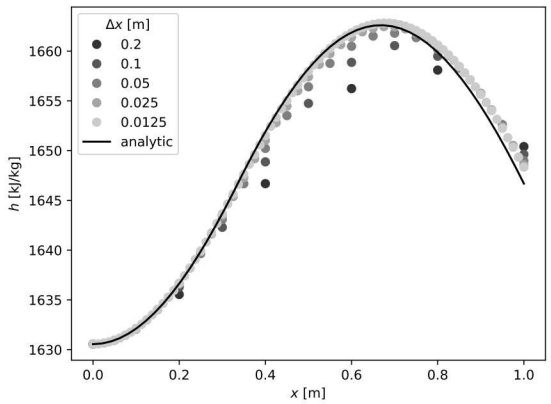

(a) Enthalpy at $t = 0.2\,\mathrm{s}$

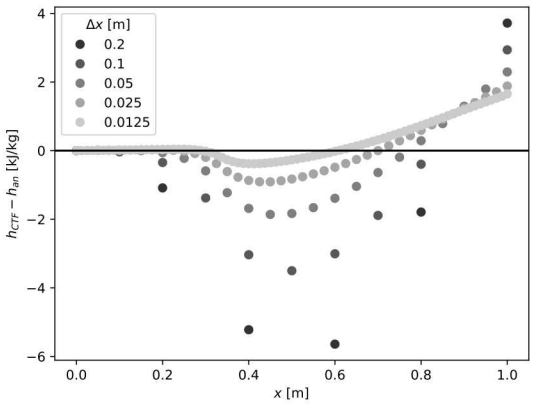

(b) Error in enthalpy at $t = 0.2\,\mathrm{s}$

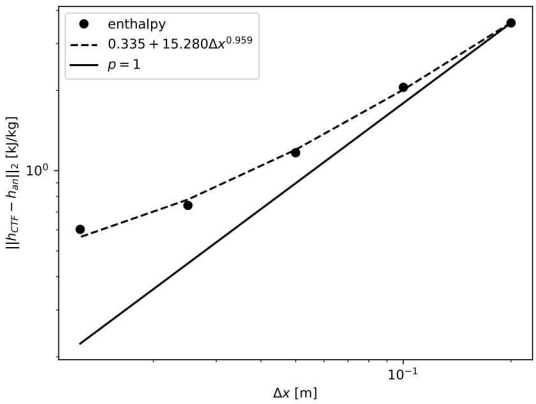

(c) Error convergence

Figure 2.9: Results for the pipe boiling verification problem

3. Unit Tests

In addition to the numerical algorithm that was verified in chapter 2, CTF contains a large number of constitutive models. These models do not display grid convergence behavior, as they account for sub-grid modeling. Therefore, these models are tested using unit tests, which verify that a call to the model has the expected output when the input is specified. The implementation of unit tests is an essential part of the SQA process. A general list of all CTF constitutive models is shown in Table 3.1. Note that two-phase, boiling, and interfacial models are currently excluded from this list, as CASL focuses on simulation of Pressurized Water Reactors (PWRs).

Remark. *CTF has many unit tests that verify geometry and other bookkeeping in the code (e.g. the coupling interface, solid and fluid mesh data structures, output processing, the iterative matrix solver). Though these types of unit tests are a vital component of SQA, they are not included in Table 3.1 as they are not evaluating constitutive models.*

Table 3.1: CTF constitutive models and corresponding unit tests. Some groups of constitutive models are excluded from this table: most multiphase models, all droplet entrainment/deentrainment models, and all noncondensible gas properties. Constitutive models are split into three groups: solid energy conservation, single phase hydraulics, and fluid energy conservation. Red check marks (✓) indicate unit tests added in this work, black check marks (✓) indicate those that already existed in the CTF testing suite.

CTF Code Capability	Model	Unit Tests
Energy Conservation in Solids		
Fuel material properties	ρ_{UO2}: constant	✓
	k_{UO2}: MATPRO-11	✓
	k_{UO2}: Modified NFI	✓
	k_{UO2}: Halden	✓
	k_{UO2}: Density correction	✓
	$c_{p,UO2}$: MATPRO-11	✓
Zircaloy material properties	ρ_{zirc}: constant	✓

	k_{zirc}: MATPRO-11	✓
	$c_{p,zirc}$: MATPRO-11	✓
Dynamic gap	H_{gas}	✓
	$H_{contact}$	✓
	H_{rad}	✓
Single Phase Hydraulics		
Equation of state	h: IAPWS	✓
	k: IAPWS	✓
	c_p: IAPWS	✓
	μ: IAPWS	✓
	σ: IAPWS	✓
	T_{sat}: IAPWS	✓
Axial/lateral wall friction	f: CTF	✓
	f: McAdams	✓
	f: Zigrang-Sylvester	✓
	f: Churchill	✓
	f: User-defined	✓
Turbulent mixing	β: Rogers and Rosehart	
	β: Beus	
Grid TKE enhancement	K/K_0: Yao, Hochreiter, and Leech	
Coolant Energy Conservation		
Wall heat transfer	Dittus-Boelter	✓
Subcooled nucleate boiling	Thom	✓
	Chen	✓
Near-wall condensation	Ahmad	✓
	Hancox-Nicoll	
Grid heat transfer enhancement	Nu/No_0: Yao, Hochreiter, and Leech	✓

All multiphase models, droplet models, and noncondensible gas properties are excluded from the table. The constitutive model matrix has about 88% coverage for single phase flow connected to a conductor. Given this outline of the generally used CTF constitutive models, there are a few notable gaps. The remainder of this chapter describes two new unit tests that are added to fill gaps in the constitutive model matrix: Dittus-Boelter and Chen.

3.1 Dittus-Boelter

The Dittus-Boelter correlation [17] is used for the heat transfer coefficient in the CTF single-phase forced convection regimes. The coded equation for Nusselt number is

$$Nu = \begin{cases} 0.023\mathrm{Re}^{0.8}\mathrm{Pr}^{0.4}, & \ell = 0 \\ \max\left[7.86, 0.023\mathrm{Re}^{0.8}\mathrm{Pr}^{0.4}\right], & \ell = 1 \\ 0, & Re = 0 \,\text{or}\, Pr = 0. \end{cases} \tag{3.1}$$

Here, ℓ indicates the variable `laminar_limit`, which determines if there is a lower limit to the Nusselt number. The constitutive model is contained in its own Fortran file, `Dittusboelter.f90`, so the implementation of a unit test is relatively simple. The tested conditions are outlined in Table 3.2. All possible combinations of behavior are tested, including passing through all combinations of `if/then/else` statements.

Table 3.2: Unit test conditions for the Dittus-Boelter constitutive model

Test	Re	Pr	`laminar_limit`	Nu
1	0	1.2		0
2	10^6	0		0
3	0	0		0
4	10^6	1.2		1560.991
5	10^3	1.2		6.214416
6	0	1.2	`.false.`	0
7	10^6	0	`.false.`	0
8	0	0	`.false.`	0
9	10^6	1.2	`.false.`	1560.991
10	10^3	1.2	`.false.`	6.214416
11	0	1.2	`.true.`	0
12	10^6	0	`.true.`	0
13	0	0	`.true.`	0
14	10^6	1.2	`.true.`	1560.991
15	10^3	1.2	`.true.`	7.860000

3.2 Chen

The Chen correlation is one option for calculating the heat transfer coefficient in the subcooled and saturated boiling regimes. The correlation is a combination of convection and nucleate boiling transfer [18].

$$q'' = (h_{NB} + h_c)(T_w - T_{sat}) \tag{3.2}$$

For this unit test, only the nucleate boiling term h_{NB} is tested. It is calculated as follows:

$$h_{NB} = 0.00122S \left[\frac{k_f^{0.79} c_{pf}^{0.45} \rho_f^{0.49}}{\sigma^{0.5} \mu_f^{0.29} h_{fg}^{0.24} \rho_g^{0.24}} \right] \Delta T_{sat}^{0.24} \Delta P_{sat}^{0.75}. \tag{3.3}$$

Here, $\Delta T_{sat} = T_w - T_{sat}$ is the wall superheat and $\Delta P = P(T_w) - P(T_{sat})$ is the difference in saturation pressure between the wall and bulk fluid. The suppression factor is presented graphically in the original paper, but is commonly approximated as

$$S = \left(1 + 0.00000253 \mathrm{Re}^{1.17}\right)^{-1}. \tag{3.4}$$

For this unit test, we employ a textbook example [19, Example 12.1]. All quantities reported in the problem definition are listen in Table 3.3 in the original units, as well as the British units necessary for use in CTF.

Table 3.3: Chen unit tests inputs from Todreas example [19]

Parameter	Symbol	SI Units	British Units
Pressure	P	7 MPa	1015.3 psi
Quality	x	0.2	0.2
Diameter	D	25 mm	0.082 ft
Mass flow rate	$\dot{m}$	800 kg/hr	1763.7 lbm/hr
Saturated water viscosity	μ_f	96×10^{-6} Pa $*$ s	0.232 lbm/ft/hr
Saturated vapor viscosity	μ_g	18.95×10^{-6} Pa $*$ s	0.046 lbm/ft/hr
Saturated water specific heat	c_{pf}	5.4×10^3 J/kg/K	1.29 btu/lbm/°F
Saturated water density	ρ_f	740 kg/m^3	46.20 lbm/ft^3
Saturated steam density	ρ_g	36.5 kg/m^3	2.28 lbm/ft^3
Surface tension	σ	18.03×10^{-3} N/m	1.235×10^{-3} lbf/ft
Heat of vaporization	h_{fg}	1513.6 kJ/kg	650.73 btu/lbm
Saturation temperature	T_{sat}	284.64 °C	544.35 °F
Wall temperature	T_w	290 °C	544 °F
Saturated water thermal conductivity	k_f	0.567 W/m/°C	0.328 btu/°F/ft/hr

The unit test is implemented to test that $h_{NB} = 1018.5$ btu/hr/ft^2/°F. First, `chen_prep` is called, then `htc_chen`. Care is taken to ensure that all unit conversions are consistent, and the `h11` variable is defined locally using the provided fluid properties.

Remark. *The heat transfer coefficient reported in [19] is* $5309\,\mathrm{W/m^2/^\circ C}$. *If his calculations are repeated to machine precision, the heat transfer coefficient becomes* $5016.6\,\mathrm{W/m^2/^\circ C}$. *However, the CTF implementation is inconsistent with the original correlation. First, the* ΔP_{sat} *term is calculated using an approximation (of unknown origin):*

$$\begin{aligned} \Delta P_{sat} &= \left[\frac{5.4042 h_{fg}}{\nu_{fg}\left(T_{sat}+460\right)}\right] \Delta T_{sat}^{A} \\ A &= \frac{1.0306}{\left(\log_{10} P\right)^{0.017}} + \frac{0.0020632}{\left(\log_{10} P\right)^{1.087}} \max\left[0, \left(\Delta T_{sat}\right) - 5\right] \end{aligned} \tag{3.5}$$

Second, the suppression factor is calculated using a different equation [20].

$$S = \begin{cases} \left[1 + 0.12 Re_{2\Phi}^{1.14}\right]^{-1} & Re_{2\Phi} < 32.5 \\ \left[1 + 0.42 Re_{2\Phi}^{0.78}\right]^{-1} & 32.5 < Re_{2\Phi} < 50.9 \\ 0.1 & 50.9 < Re_{2\Phi} \end{cases} \tag{3.6}$$

When these two modifications are incorporated into Todreas' solution, the result is $5779.4\,\mathrm{W/m^2/^\circ C}$ *(*$1018.5\,\mathrm{btu/hr/ft^2/^\circ F}$*), which is the value tested in the CTF unit test. This value is about 15% from the hand calculated value without these modifications.*

4. Conclusion

In this work, some code verification studies were performed for the NCSU/CASL version of COBRA-TF. New tests were incorporated into the CTF automated regression suite: isokinetic advection [6], linear conduction [7], friction and gravity, convection, and pipe boiling. These problems, along with the existing heat exchanger problem, were incorporated into a common Python utility that generalizes the verification process. The python utility will enable quick implementation and testing of any future code verification studies for CTF. For each test, the computed solution is compared to an analytic solution as the code mesh is refined. All code behavior for these problems is consistent with expected results, indicating a lack of code bugs in the exercised sections of the code. In addition, two problems were examined that were not added to the automated regression suite: water faucet [8] and nonlinear conduction. For both of these tests, the results were promising, but future work will be necessary to troubleshoot and finalize them.

The CTF automated regression suite currently contains ten code convergence studies. Though this is an improvement over the pre-CASL version of the code, it is far from complete. First, there are gaps to address in Table 1.1. Some terms have no corresponding verification tests: lateral advection and turbulent mixing of mass, lateral advection of energy, interfacial shear, and turbulent mixing of momentum. Many of these gaps could easily be filled using modifications of the existing turbulent mixing and flow split problems. For terms that already have corresponding tests in Table 1.1, many other problems could be added to increase the confidence in that particular term. In addition, future work should focus on testing *different combinations* of terms in the conservation equations, rather than testing individual terms. It is possible that the interplay between two different terms could reveal a code bug that is not observed when only the individual terms are tested.

Finally, future work will also include solution verification analyses. There are a handful of solution verification studies relevant to CTF in the literature, but none of them are included in the CTF automated regression suite. A more inclusive and thorough solution verification study will be necessary to quantify the numerical error when all CTF constitutive models are enabled.

In addition to the code verification studies completed in this work, a few unit tests were added to address gaps in the constitutive model matrix. The two models with new tests are the Dittus-Boelter and Chen

correlations. Some models in Table 3.1, such as Beus and Rogers-Rosehart, are calculated in the middle of very large Fortran modules. It is very difficult to individually test the behavior of these models. Therefore, to further enable future unit testing activities, these constitutive models should be migrated to their own Fortran functions.

Acknowledgments

Thanks to Vincent Mousseau, Lindsay Gilkey, and Aaron Krueger of Sandia National Laboratories for their thoughtful reviews.

Sandia National Laboratories is a multi-program laboratory managed and operated by National Technology and Engineering Solutions of Sandia, LLC, a wholly owned subsidiary of Honeywell International, for the U.S. Department of Energy's National Nuclear Security Administration under contract DE-NA0003525. This research is supported by and performed in conjunction with the Consortium for Advanced Simulation of Light Water Reactors (`http://www.casl.gov`), an Energy Innovation Hub (`http://www.energy.gov/hubs`) for Modeling and Simulation of Nuclear Reactors under US Department of Energy Contract No. DE-AC05-00OR22725.

This paper describes objective technical results and analysis. Any subjective views or opinions that might be expressed do not necessarily represent the views of the U.S. Department of Energy or the United States Government.

Bibliography

[1] M. J. Thurgood et al. *COBRA/TRAC: A Thermal-Hydraulics Code for Transient Analysis of Nuclear Reactor Vessels and Primary Coolant Systems*. Tech. rep. NUREG/CR-3046, PNL-4385. https://www.nrc.gov/docs/ML0703/ML070320229.pdf. US Nuclear Regulatory Commission, 1983.

[2] W. L. Oberkampf, M. Pilch, and T. G. Trucano. *Predictive Capability Maturity Model for Computational Modeling and Simulation*. Tech. rep. SAND2007-5948. Sandia National Laboratories (SNL), 2007.

[3] W. L. Oberkampf and C. J. Roy. *Verification and Validation in Scientific Computing*. first. Cambridge, UK: Cambridge University Press, 2010.

[4] T. G. Trucano et al. "Calibration, Validation, and Sensitivity Analysis: What's What". In: *Reliab. Eng. Syst. Saf.* 91 (2006), pp. 1131–1357. DOI: 10.1016/j.ress.2005.11.031.

[5] R. Salko et al. *CTF Validation and Verification Manual*. Tech. rep. CASL-U-2019-1887. CASL, 2019.

[6] N. Porter, V. Mousseau, and M. Avramova. "Solution Verification of CTF and CTF-R Using Isokinetic Advection Test Problems". In: *International Conference on Mathematics and Computational Methods Applied to Nuclear Science and Engineering (M&C-2017)*. Jeju, Korea, Apr. 2017.

[7] A. Toptan et al. "A new fuel modeling capability, CTFFuel, with a case study on fuel thermal conductivity degredation". In: *Nuclear Engineering and Design* 341 (2019), pp. 248–258. DOI: 10.1016/j.nucengdes.2018.11.010.

[8] M. G. Delchini, R. K. Salko, and V. A. Mousseau. "Implementation of a Pressure Correction Term in the CTF Sub-Channel Code". In: *ANS Annual Meeting*. San Franciso, CA, June 2017.

[9] V. H. Ransom. "Numerical Benchmark Tests". In: *Multiphase Science and Technology*. Ed. by G. F. Hewitt, J. M. Delhaye, and N. Zuber. Vol. 2. John Wiley & Sons Ltd, 1987.

[10] J. W. Banks, T. Aslam, and W. J. Rider. "On Sub-Linear Convergence for Linearly Degenerate Waves in Capturing Schemes". In: *Journal of Computational Physics* 227 (2008), pp. 6985–7002. DOI: 10.1016/j.jcp.2008.04.002.

[11] T. G. Theofanous and W. H. Amarasooriya. "Physical Benchmarking Exercises". In: *Multiphase Science and Technology*. Ed. by G. F. Hewitt, J. M. Delhaye, and N. Zuber. Vol. 6. John Wiley & Sons Ltd, 1992.

[12] L. Zou, H. Zhao, and H. Zhang. "New Analytical Solutions to the Two-Phase Water Faucet Problem". In: *Progress in Nuclear Energy* 91 (2016), pp. 389–398. DOI: 10.1016/j.pnucene.2016.05.013.

[13] J. D. Ramshaw and J. A. Trapp. "Characteristics, Stability, and Short-Wavelength Phenomena in Two-Phase Flow Equation Systems". In: *Nuclear Science and Engineering* 66.1 (1978), pp. 93–102. DOI: 10.13182/NSE78-A15191.

[14] J. H. Stuhmiller. "The Influence of Interfacial Pressure on the Character of the Two-Phase Flow Model Equations". In: *International Journal of Multiphase Flow* 3.6 (1977), pp. 511–560. DOI: 10.1016/0301-9322(77)90029-5.

[15] A. Toptan et al. "Implementation and Assessment of Wall Friction Models for LWR Core Analysis". In: *Annals of Nuclear Energy* 115 (2018), pp. 565–572. DOI: 10.1016/j.anucene.2018.02.022.

[16] M. Jakob. *Heat Transfer*. New York, NY: Wiley, 1949.

[17] F. W. Dittus and L. M. K. Boelter. "Heat Transfer in Automobile Radiators of the Tubular Type". In: *Publications in Engineering 2*. University of California, Berkeley, 1930, pp. 443–461. DOI: 10.1016/0735-1933(85)90003-X.

[18] J. C. Chen. "Correlation for Boiling Heat Transfer to Saturated Fluids in Convective Flow". In: *Industrial Engineering Chemistry Process Design and Development* 5.3 (1966). DOI: 10.1021/i260019a023.

[19] N. E. Todreas and M. S. Kazimi. *Nuclear Systems Volume I: Thermal Hydraulic Fundamentals*. Second. Boca Raton, FL: Taylor & Francis, 2012.

[20] T. A. Bjornard and P. Griffith. "PWR Blowdown Heat Transfer". In: *Thermal and Hydraulic Aspects of Nuclear Reactor Safety*. Vol. 1. American Society of Mechanical Engineers. 1977, pp. 17–41.